

## Dominant Imprint of Rossby Waves in the Climate Network

Yang Wang,<sup>1,\*</sup> Avi Gozolchiani,<sup>2,3</sup> Yosef Ashkenazy,<sup>3</sup> Yehiel Berezin,<sup>1</sup> Oded Guez,<sup>1</sup> and Shlomo Havlin<sup>1,†</sup>

<sup>1</sup>*Department of Physics, Bar-Ilan University, Ramat-Gan 52900, Israel*

<sup>2</sup>*Institute of Earth Sciences, The Hebrew University of Jerusalem, Jerusalem 91904, Israel*

<sup>3</sup>*Department of Solar Energy and Environmental Physics, BIDR, Ben-Gurion University, Midreshet Ben-Gurion 84990, Israel*

(Received 31 March 2013; published 24 September 2013)

The connectivity pattern of networks based on ground level temperature records shows a dense stripe of links in the extra tropics of the southern hemisphere. We show that statistical categorization of these links yields a clear association with the pattern of an atmospheric Rossby wave, one of the major mechanisms associated with the weather system and with planetary scale energy transport. It is shown that alternating densities of negative and positive links are arranged in half Rossby wave distances around 3500, 7000, and 10 000 km and are aligned with the expected direction of energy flow, distribution of time delays, and the seasonality of these waves. In addition, long distance links that are associated with Rossby waves are the most dominant in the climate network.

DOI: [10.1103/PhysRevLett.111.138501](https://doi.org/10.1103/PhysRevLett.111.138501)

PACS numbers: 92.60.hv, 05.40.-a, 89.60.-k, 92.60.Bh

Networks have become an important tool for analyzing technological and natural systems [1–4], including social relations [5], biochemical interactions [6–8], information flow through the world wide web [9], physiological activities [10], and the mitigation of attacks on transportation infrastructures [11]. It was suggested recently that climate variables can be viewed as a climate network [12–20] where different regions of the world are regarded as nodes and communications between different locations via, e.g., heat and material exchange are regarded as links. A multitude of statistical analysis methods is often used to capture major variability patterns in climate time series [21–23], where the correlation matrix plays an important part. The climate network provides a complementary tool to study the statistical properties of the climate system.

The climate network often has very strong links, which are caused by a proximity (distance) effect [17]. Namely, pairs of sites close to each other (below  $\sim 2000$  km) are often strongly positively correlated. A significant fraction of the stable network structure may be associated with the proximity effect. It is hence common to analyze climate time series also based on negative correlations (e.g., Refs. [24–26]), which usually represent more interesting remote interactions, called teleconnections.

However, recent studies have not distinguished between positive and negative correlations in climate networks [10,13–20]. Apparently, a large fraction of the network links resides in the southern ocean [14,15,18]. These links possibly include (beyond the proximity effect distance) both negative and positive correlations.

Here we analyze separately the negative and positive correlations of the climate network. We show that the correlations of these links alternate, as a function of distance, between negative and positive, consistent with a wave pattern. We find that the time delay associated with these links increases from one to five days as a function of

the distance between the nodes. We also analyze the typical length scale of the links, their seasonality, and the geographical structure of the climate network and find that these are consistent with atmospheric Rossby waves [27], one of the most efficient mechanisms of planetary-scale energy transfer.

Rossby waves are known to have a major role in initiating low pressure systems that influence the daily weather conditions. These waves exist due to the variation of the Coriolis force with latitude. They bear a special characteristic as they always propagate westward in the absence of background flow. The fastest Rossby waves are the longest ones and their wavelength is of the order of planetary scales. The zonal phase speed of long Rossby waves is independent of the wave number and is thus equal to the zonal group velocity making long Rossby waves nondispersive.

Studies of atmospheric Rossby waves are usually based on 300 hPa meridional wind velocity reanalysis data [28–30]. Here we show that it is possible to uncover the characteristics of Rossby waves using more common and reliable surface data, like surface air temperature. We find that Rossby waves dominate the climate network, an observation that, surprisingly, has not been previously reported.

We analyze the daily data of air temperature, sea level pressure, geopotential height, and meridional velocity reanalysis fields [31], mapped to a network of 726 nodes around the globe (small dots in Fig. 4) [32]. Below, we mainly focus on the surface temperature field as one of the most common and reliable types of data. For each node (i.e., longitude-latitude grid point), daily values within the period 1948–2010 are used, from which we extract anomaly values. Specifically, given a record  $\tilde{T}^y(d)$ , where  $y$  is the year and  $d$  is the day (from 1 to 365), then the filtered record is defined as  $T^y(d) = \tilde{T}^y(d) - (1/N)\sum_y \tilde{T}^y(d)$ ,

where  $N$  is the total number of years. We also define  $\Theta_s^y(d) \equiv [T_s(d) - \langle T_s(d) \rangle] / \langle (T_s(d) - \langle T_s(d) \rangle)^2 \rangle^{1/2}$ , where  $\langle \cdot \cdot \rangle$  is the average of the time series.

The link between each pair of sites on the grid  $s_1$  and  $s_2$  is calculated as the cross-correlation function  $X_{s_1, s_2}^y(\tau \geq 0) = \langle \Theta_{s_1}^y(d) \Theta_{s_2}^y(d + \tau) \rangle$ , where  $\tau$  is the time lag and  $X_{s_1, s_2}^y(\tau) = X_{s_2, s_1}^y(-\tau)$ . We define the time lag  $\tau^*$  at which  $X_{s_1, s_2}^y(\tau)$  is maximal (or minimal), as the time delay of a pair  $s_1, s_2$ . When  $s_1$  is to the west of  $s_2$  and the time lag is positive, the link direction is to the east. We distinguish between positive and negative link weights as follows:

$$W_{s_1, s_2}^y = \frac{\max(X_{s_1, s_2}^y) - \text{mean}(X_{s_1, s_2}^y)}{\text{std}(X_{s_1, s_2}^y)}, \quad (1)$$

and

$$W_{s_1, s_2}^y = \frac{\min(X_{s_1, s_2}^y) - \text{mean}(X_{s_1, s_2}^y)}{\text{std}(X_{s_1, s_2}^y)}, \quad (2)$$

where max and min are the maximum and minimum values of the cross-correlation function, mean and std are the mean and standard deviation, and  $y$  denotes a specific year. Typical time series and their cross-correlation functions are shown in Fig. 1, where the absolute value of a minimal (negative) cross-correlation function is much larger than the maximal value.

We implemented the above procedure for winter and summer time series. We calculate the cross-correlation functions of each pair of sites, where the data ranges from May 1st to August 31st (123 days) for the southern hemisphere (SH) winter or from November 1st to February 28th (120 days) for the SH summer. We choose a maximal time lag of 72 days. The correlation coefficient is based on

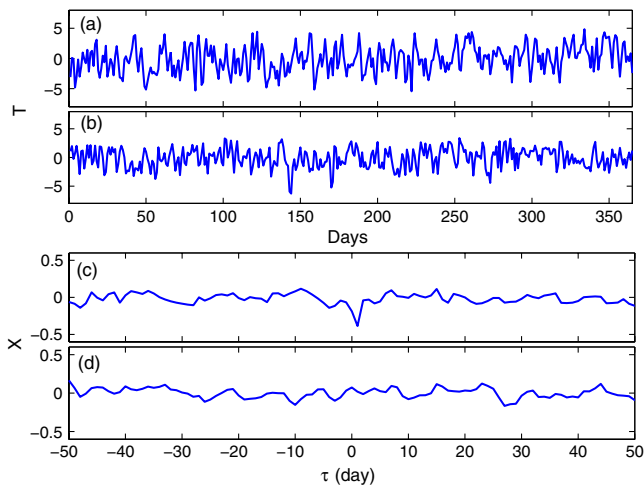


FIG. 1 (color online). (a) An example of a seasonally detrended surface temperature daily time series from  $45^\circ\text{S}$ ,  $52.5^\circ\text{E}$  for the year 1948. (b) Same as (a) for  $45^\circ\text{S}$ ,  $97.5^\circ\text{E}$ . (c) The cross-correlation function between the time series shown in (a) and (b). (d) Same as (c) but when the time series of the two sites are of different years (“shuffling” method).

12 months of data to have sufficient statistics. This is done by “gluing” three consecutive winters (summers). Similar analysis based on four periods of three months yielded results which are consistent with all the following.

We analyze a near surface (1000 hPa) temperature time series. First, we focus on the properties of link weight around the globe (see Fig. 2) for the months November to February. To identify the significant links we apply a shuffling procedure in which the order of the years is shuffled while the order within each year remains unchanged. This shuffling preserves all the statistical quantities of the data, such as the distribution of values and their autocorrelation properties, making the nodes independent. Figures 2(a) and 2(b) depict the link-weight statistics for the real and shuffled data. High negative mean-link-weight values exist in the probability density function (PDF) of the real data but not in the shuffled data, and therefore are not likely to occur by chance. Moreover, high variability (std.) during different years of the time delays of links  $\tau^*$  is also a signature of random behavior [10] [see Fig. 2(b)]. The differences between the distribution of real data and shuffled data indicate that many significant negative links exist in the climate network [see Figs. 2(a) and 2(b)]. We obtain similar results for positive links and other fields (not shown).

Next, we divide the world into three geographical zones, the SH ( $22.5^\circ\text{S}$ – $90^\circ\text{S}$ ), the northern hemisphere (NH) ( $22.5^\circ\text{N}$ – $90^\circ\text{N}$ ), and the equator ( $22.5^\circ\text{S}$ – $22.5^\circ\text{N}$ ). We then calculate the (geographical and temporal) mean link weight  $\langle W_{s_1, s_2} \rangle$  as a function of the geographical distance of links  $d$ . It is clear that in the SH, there is a preferred distance of  $\sim 3500$  km and a weaker one of  $\sim 10000$  km [see Fig. 2(c)]. In the NH region, we find a similar, weaker distance dependence, while in the equatorial region, there is no preferred distance [see Fig. 2(c)]. These preferred distances may be associated with atmospheric Rossby waves (eddies) [28–30,33], which have a wavelength of  $\sim 7000$  km and which are known to be pronounced in the SH, weaker in the NH, and absent in the equatorial region [29,30]. The negative peaks at 3500 and 10000 km represent  $1/2$  and  $3/2$  wavelengths of the observed Rossby wavelength.

To consolidate the association of the observed climate network pattern with Rossby waves, we compare the seasonality of this pattern with the known seasonal characteristics of Rossby waves. In Figs. 3(a)–3(d), we plot the negative and positive weights of all SH links, for the winter and summer. Each point represents an average link weight  $\langle W \rangle$  over years versus its distance  $d$ . The negative weights [Eq. (2)] have a pronounced distribution of large weights for  $d \sim 3500$  km during both summer and winter, while for the SH summer (November to February), there is an additional preferred distance of  $\sim 10000$  km [see Fig. 3(b)], both in accordance with the  $1/2$  and  $3/2$  wavelengths of atmospheric Rossby waves. Around the full wavelength

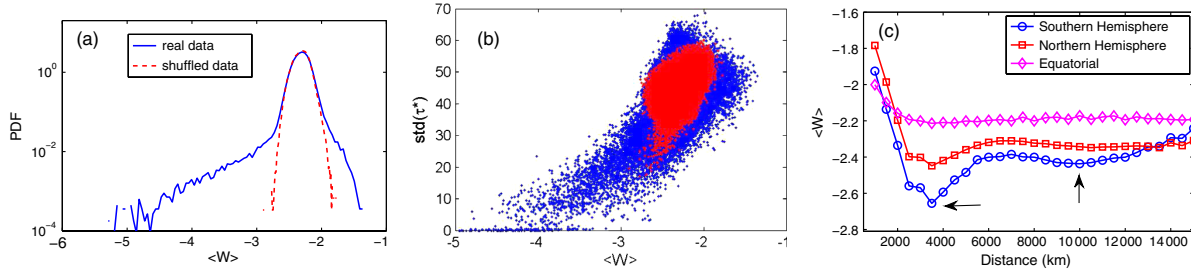


FIG. 2 (color online). (a) The PDF of the mean weight of negative links in the globe, in real (solid line) and shuffled (dashed line) data. (b) The dependence of the std. of time delay  $\tau^*$  on the mean weight ( $W$ ) for all possible links, for real [dark gray (blue)] and shuffled [light gray (red)] data. (c) The mean negative link weight as a function of distance  $d$ , for the SH (circles), the NH (squares), and the equatorial (diamonds) regions. The figure is based on the globe temperature records at 1000 hPa isobar for November to February.

distance (i.e.,  $d \sim 7000$  km), we find, as expected, an enhanced distribution of large positive weights [Eq. (1)] [see Figs. 3(c) and 3(d)]. However, a clearer wave pattern is observed during summer (represented by links at  $1/2$ , 1, and  $3/2$  wavelengths) in comparison to winter [see Figs. 3(a)–3(d)], in agreement with the clearer pattern of Rossby waves found in the SH during the SH summer [28–30]. The situation is similar in the NH (not shown), for

the NH winter. In the distribution of positive weights [see Figs. 3(c) and 3(d)], one clearly sees the links that emerge around  $d < 2000$  km due to the proximity effect.

Atmospheric Rossby waves have a characteristic group velocity, and we now estimate it based on the results shown above. We thus divide  $d$  by  $\tau^*$  for each link, assuming that  $\tau^*$  estimates the underlying dynamical delay between the two sites (nodes) [34]. Since  $\tau^*$  is only meaningful for links with weights above the background noise level (see Fig. 2(b) and Ref. [17]), we limit the analysis to links with weights  $|\bar{W}| > 2.8$  [35]. Furthermore, to avoid links that are prone to the proximity effect (relevant for the current Rossby wave interpretation), when considering positively correlated links, we consider links with  $d > 5000$  km. Also, we constrain the near negative links to be within  $d \in [2000, 5000]$  km and far negative links to have  $d > 8000$  km. The PDFs of time delay  $\tau^*$  of the near negative links, the far positive links, and the far negative

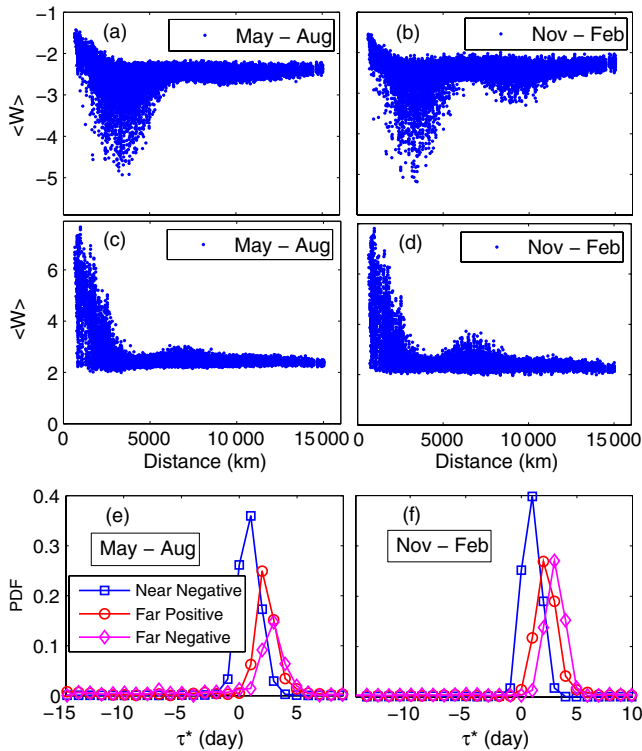


FIG. 3 (color online). The dependence of the weight of negative links on the distance  $d$  in the SH during (a) winter and (b) summer. (c),(d) Same as (a),(b) for positive links. The PDF of time delays  $\tau^*$  of near negative (squares,  $d \sim 3500$  km), far positive (circles,  $d \sim 7000$  km), and far negative (diamonds,  $d \sim 10000$  km) weighted links, in the SH during (e) winter and (f) summer.

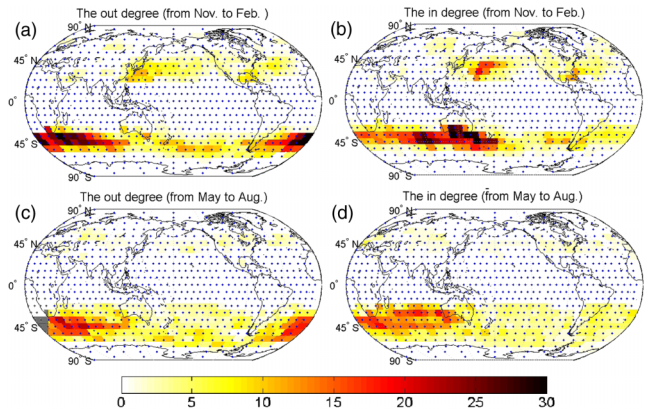


FIG. 4 (color online). The out degree (a) and in degree (b) of the climate network structure from November to February (SH summer). The out degree (c) and in degree (d) of the climate network structure from May to August (SH winter). The specific region of outgoing and incoming links indicates eastward “network flow,” similar to Rossby waves traveling on top of an eastward jet.

links are shown in Figs. 3(e) and 3(f). By our convention, positive  $\tau^*$  means an eastward energy flow, a typical case for most observed links. The approximated time lag is  $\tau \approx 1$  day for the near negative links [i.e., links in the first peak in Fig. 3(a)],  $\tau \approx 2-3$  days for the far (beyond the proximity effect) positive links, and  $\tau \approx 3-4$  days for the far negative links [second peak of Figs. 3(a) and 3(b)]. These lead to estimated group velocities of 20–35 m/s, consistent with the previously reported [30,36] velocities of 23–32 m/s.

The embedding of the climate network in real space enforces a latticelike topology merged with a set of long-ranged links. The short geometrical distance links are due to the proximity effect, and the links that approach larger distances and break the Euclidean order are due to integer numbers of half wavelengths of Rossby waves. To directly show this, we calculate the distribution of geometrical distances associated with network distances (i.e., minimal number of links connecting pairs of nodes) of 1–4. The network distance 1 case is already depicted in Fig. 2(c). For network distance 2 the geographical distances are distributed around one Rossby wave wavelength during the SH winter, and  $3/2$  Rossby wave wavelengths during the SH summer (see Fig. 1 in the Supplemental Material [37]). Thus, network distance 2 corresponds to a composition of integral numbers of half Rossby wave wavelengths. This scenario suggests a network topology similar to Ref. [38], known as small world (see the Supplemental Material [37]).

The climate network has a unique geographical structure that can be compared with the geographical structure of Rossby waves. Since the network is directed—positive  $\tau$  indicates eastward flow while negative  $\tau$  indicates westward flow—we distinguish between a link that is pointing toward a node (where the number of links pointing to a specific node is referred to below as “in degree”), or away from the node (referred to below as “out degree”) (see Ref. [18]). Figure 4 depicts the mean in and out degrees of each node, excluding the equatorial region (as it is not related to the current discussion). The observed structure is consistent with the structure of Rossby waves (eddies) [30]. First, the wave band in the SH for the SH winter [see Figs. 4(c) and 4(d)] is broader than that of the SH summer [see Figs. 4(a) and 4(b)]. Second, the atmospheric Rossby wave structure in the NH summer is less pronounced. Third, the wave structure in the SH summer lies on a band centered near  $50^\circ\text{S}$ . Fourth, the transient heat flux (usually used to map storm tracks that are influenced by Rossby waves [39] (see Fig. 4 in the Supplemental Material [37]) and the network pattern of Fig. 4 are qualitatively similar. All the above characteristics are consistent with the properties of Rossby waves.

Previous studies found the 300 hPa meridional velocity field to be the most suitable for studying the characteristics of Rossby waves [28–30]. Our method captures the wave properties also using other fields at various altitudes. In

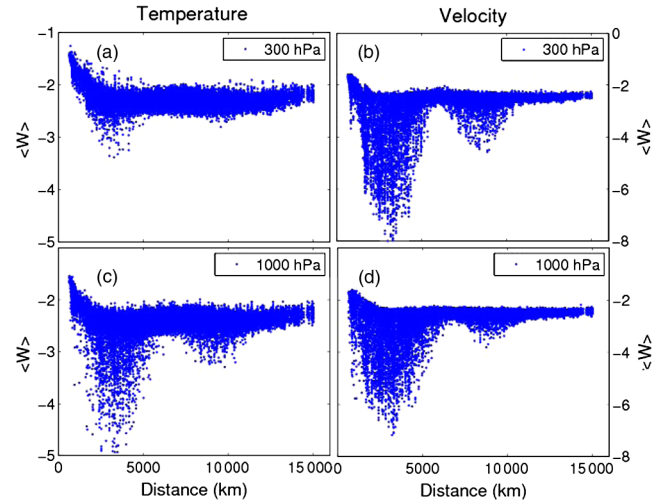


FIG. 5 (color online). The dependence of the weight of negative links on the distance  $d$  in the SH during the SH summer months for temperature (left panels) and meridional velocity (right panels) for 300 hPa (upper panels) and 1000 hPa (lower panels).

particular, we showed above that the wave pattern is clearly seen at a ground level (1000 hPa) temperature field, a more common and reliable variable. In Fig. 5, we compare, using the climate network technique, the mean weight distributions of the negative links of the meridional velocity and temperature fields. We find that the pattern of the two fields is similar, although the meridional velocity yields larger weights. Additionally, the meridional velocity yields a clearer pattern at the high altitude of 300 hPa, while the temperature field yields a clearer pattern at the ground level of 1000 hPa.

In summary, we analyzed the properties of the climate network by considering, separately, positive and negative correlations (links). The most dominant links in the climate network with a geographical distance larger than 2000 km are found for distances of  $\sim 3500$ ,  $\sim 7000$ , and  $\sim 10000$  km, coinciding with the  $1/2$ , 1, and  $3/2$  wavelengths of common atmospheric Rossby waves. Moreover, the time delays associated with these distances coincide with the direction of the energy flow and with the group velocity of the atmospheric Rossby waves. The pronounced length scales of the climate network, the dominance in the SH relative to the NH, and the dominance during the SH summer in the SH are all consistent with the properties of atmospheric Rossby waves. All of these factors thus provide strong support for the association of the majority of the climate network far links with Rossby waves. This association of Rossby waves with a certain regime of links in the climate network can now be used to bridge between the network analysis and the climate system. This may turn out to be useful for climate problems related to real and model data (see e.g. Ref. [40]) in which conventional approaches are exhausted.

We thank the LINC project (No. 289447) funded by the EC's Marie-Curie ITN program (FP7-PEOPLE-2011-ITN) and the Israel Science Foundation for financial support. We thank Edmund Chang and Nili Harnik for helpful insights regarding Rossby waves. Y.W. thanks the China Scholarship Council (CSC) for support.

\*wangyang.maple@gmail.com

†havlin@ophir.ph.biu.ac.il

- [1] R. Albert and A.-L. Barabasi, *Rev. Mod. Phys.* **74**, 47 (2002).
- [2] S. Boccaletti, V. Latora, Y. Moreno, M. Chavez, and D.-U. Hwang, *Phys. Rep.* **424**, 175 (2006).
- [3] M.E.J. Newman, *Networks: An Introduction* (Oxford University, New York, 2010).
- [4] R. Cohen and S. Havlin, *Complex Networks: Structure, Robustness and Function* (Cambridge University Press, Cambridge, England, 2010).
- [5] M. Girvan and M.E.J. Newman, *Proc. Natl. Acad. Sci. U.S.A.* **99**, 7821 (2002).
- [6] R. Guimera and L.A.N. Amaral, *Nature (London)* **433**, 895 (2005).
- [7] G. Palla, I. Derenyi, I. Farkas, and T. Vicsek, *Nature (London)* **435**, 814 (2005).
- [8] H. Jeong, B. Tombor, R. Albert, Z.N. Oltvai, and A.-L. Barabasi, *Nature (London)* **407**, 651 (2000).
- [9] B.A. Huberman, *The Laws of the Web* (MIT, Cambridge, MA, 2001).
- [10] A. Bashan, R. P. Bartsch, J. W. Kantelhardt, S. Havlin, and P. Ch. Ivanov, *Nat. Commun.* **3**, 702 (2012).
- [11] C.M. Schneider, A.A. Moreira, J.S. Andrade, Jr., S. Havlin, and H.J. Herrmann, *Proc. Natl. Acad. Sci. U.S.A.* **108**, 3838 (2011).
- [12] J. Ludescher, A. Gozolchiani, M.I. Bogachev, A. Bunde, S. Havlin, and H.J. Schellnhuber, *Proc. Natl. Acad. Sci. U.S.A.* **110**, 11 742 (2013).
- [13] A. A. Tsonis, K. L. Swanson, and P. J. Roebber, *Bull. Am. Meteorol. Soc.* **87**, 585 (2006).
- [14] K. Yamasaki, A. Gozolchiani, and S. Havlin, *Phys. Rev. Lett.* **100**, 228501 (2008).
- [15] A. A. Tsonis and K. L. Swanson, *Phys. Rev. Lett.* **100**, 228502 (2008).
- [16] J. F. Donges, Y. Zou, N. Marwan, and J. Kurths, *Europhys. Lett.* **87**, 48007 (2009).
- [17] Y. Berezin, A. Gozolchiani, O. Guez, and S. Havlin, *Sci. Rep.* **2**, 666 (2012).
- [18] A. Gozolchiani, S. Havlin, and K. Yamasaki, *Phys. Rev. Lett.* **107**, 148501 (2011).
- [19] O. Guez, A. Gozolchiani, Y. Berezin, S. Brenner, and S. Havlin, *Europhys. Lett.* **98**, 38006 (2012).
- [20] J. F. Donges, Y. Zou, N. Marwan, and J. Kurths, *Eur. Phys. J. Special Topics* **174**, 157 (2009).
- [21] H. V. Storch and F. W. Zwiers, *Statistical Analysis in Climate Research* (Cambridge University Press, Cambridge, England, 2003).
- [22] L. F. Robinson, V. H. de la Pena, and Y. Kushnir, *Theor. Appl. Climatol.* **94**, 215 (2008).
- [23] P. Alpert and T. Sholokhman, *Factor Separation in the Atmosphere: Applications and Future Prospects* (Cambridge University Press, Cambridge, England, 2011).
- [24] J. M. Wallace and D. S. Gutzler, *Mon. Weather Rev.* **109**, 784 (1981).
- [25] B. J. Hoskins and D. Karoly, *J. Atmos. Sci.* **38**, 1179 (1981).
- [26] G. T. Walker, *Q.J.R. Meteorol. Soc.* **51**, 337 (1925).
- [27] These waves are sometimes called “generalized Rossby waves” or simply “baroclinic waves,” to express their deviation from barotropic Rossby waves. That is, the fields here are nonuniform across different altitudes.
- [28] E. K. M. Chang, *J. Atmos. Sci.* **50**, 2038 (1993).
- [29] E. K. M. Chang and B. Y. Daniel, *J. Atmos. Sci.* **56**, 1708 (1999).
- [30] E. K. M. Chang, *J. Atmos. Sci.* **56**, 1729 (1999).
- [31] E. Kalnay *et al.*, *Bull. Am. Meteorol. Soc.* **77**, 437 (1996); PSD Gridded Climate Datasets, <http://www.esrl.noaa.gov/psd/data/gridded/>.
- [32] The original resolution of the reanalysis data is 2.5°. The number of nodes that were analyzed was normalized by the cosine of latitude to keep the density of nodes equally distributed.
- [33] E. K. M. Chang, *J. Atmos. Sci.* **62**, 2467 (2005).
- [34] L. Cimponeriu, M. Rosenblum, and A. Pikovsky, *Phys. Rev. E* **70**, 046213 (2004).
- [35] We have checked thresholds in the range 2.7–3 without significant qualitative changes in the results.
- [36] E. H. Berbery and C. S. Vera, *J. Atmos. Sci.* **53**, 468 (1996).
- [37] See Supplemental Material at <http://link.aps.org/supplemental/10.1103/PhysRevLett.111.138501> for additional information regarding the network topology, and the storm track pattern similar to our network pattern.
- [38] D. J. Watts and S. H. Strogatz, *Nature (London)* **393**, 440 (1998).
- [39] Y. Ashkenazy, Y. Feliks, H. Gildor, and E. Tziperman, *J. Atmos. Sci.* **65**, 3327 (2008).
- [40] CMIP: Coupled Model Intercomparison Project, <http://cmip-pcmdi.llnl.gov>.